Contents lists available at ScienceDirect

Biomaterials

Efficient production and enhanced tumor delivery of engineered extracellular vesicles

CrossMark

Dionysios C. Watson [a], Defne Bayik [b, c, 1], Avinash Srivatsan [d, 1], Cristina Bergamaschi [e], Antonio Valentin [a], Gang Niu [d], Jenifer Bear [e], Mitchell Monninger [f], Mei Sun [f], Aizea Morales-Kastresana [g], Jennifer C. Jones [g], Barbara K. Felber [e], Xiaoyuan Chen [d], Ihsan Gursel [c], George N. Pavlakis [a, *]

[a] Human Retrovirus Section, Vaccine Branch, Center for Cancer Research, National Cancer Institute at Frederick, Frederick, MD 21702, United States
[b] Cancer and Inflammation Program, Center for Cancer Research, National Cancer Institute at Frederick, Frederick, MD 21702, United States
[c] Department of Molecular Biology and Genetics, Bilkent University, Ankara, 06800 Turkey
[d] Laboratory of Molecular Imaging and Nanomedicine, National Institute of Biomedical Imaging and Bioengineering, National Institutes of Health, Bethesda, MD 20892, United States
[e] Human Retrovirus Pathogenesis Section, Vaccine Branch, Center for Cancer Research, National Cancer Institute at Frederick, Frederick, MD 21702, United States
[f] Pathology Division, United States Army Medical Research Institute of Infectious Diseases, Frederick, MD 21702, United States
[g] Vaccine Branch, Center for Cancer Research, National Cancer Institute, Bethesda, MD 20892, United States

ARTICLE INFO

ABSTRACT

Extracellular vesicles (EV), including exosomes and microvesicles, are nano-sized intercellular communication vehicles that participate in a multitude of physiological processes. Due to their biological properties, they are also promising candidates for the systemic delivery of therapeutic compounds, such as cytokines, chemotherapeutic drugs, siRNAs and viral vectors. However, low EV production yield and rapid clearance of administered EV by liver macrophages limit their potential use as therapeutic vehicles. We have used a hollow-fiber bioreactor for the efficient production of bioactive EV bearing the heterodimeric cytokine complex Interleukin-15:Interleukin-15 receptor alpha. Bioreactor culture yielded ~40-fold more EV per mL conditioned medium, as compared to conventional cell culture. Biophysical analysis and comparative proteomics suggested a more diverse population of EV in the bioreactor preparations, while serum protein contaminants were detectable only in conventional culture EV preparations. We also identified the Scavenger Receptor Class A family (SR-A) as a novel monocyte/macrophage uptake receptor for EV. In vivo blockade of SR-A with dextran sulfate dramatically decreased EV liver clearance in mice, while enhancing tumor accumulation. These findings facilitate development of EV therapeutic methods.

1. Introduction

Extracellular vesicles (EV), including exosomes and microvesicles, are nano-sized membrane vesicles secreted by most cell types. Given their intrinsic properties, e.g. immunomodulation [1,2] and their ability to distribute systemically, EV are being developed as biocompatible, targeted therapeutic particles [3,4]. Techniques

to load bioactive cargo, such as protein [5,6], siRNA [7], viral vectors [8], and chemotherapeutics [9] are also currently investigated in several settings.

EV for therapeutic applications are typically purified from cell culture conditioned media of cell lines or primary cells. Purification methods are comprised of combinations of techniques, including ultracentrifugation, filtration, precipitation, and chromatography [10—12], each resulting in somewhat different mixtures of EV species and non-EV contaminants. Reported EV yields range from 1 to 10 μg/mL culture supernatant, even from "high-yield" systems, such as the Integra CELLine bioreactor [7,13,14]. Thus, obtaining sufficient material for in vivo studies currently comprises a

* Corresponding author.
  E-mail address: George.pavlakis@nih.gov (G.N. Pavlakis).
[1] These authors contributed equally to the work.

technical bottleneck for therapeutic EV development, irrespective of the purification method.

With regard to systemic delivery of EV, modifying surface proteins with targeting ligands has enabled increased delivery to the CNS (via the RGD targeting peptide) [3] and to EGFR-expressing tumors (via the GE11 peptide) [15]. However, systemically delivered EV are rapidly cleared by the monocyte/macrophage or reticuloendothelial system (RES), resulting in minimal accumulation within the desired target sites [4,15–19], which is a major hurdle for EV-based systemic therapeutic approaches. Depletion of monocytes/macrophages was shown to significantly prolong EV systemic half-life in mice, suggesting uptake by these cells as an important mechanism of EV clearance in vivo [17]. Clearance of synthetic nanoparticles by the RES was shown to be largely mediated by the Scavenger Receptor Class A family (SR-A), which recognizes a variety of negatively charged ligands, including phosphatidylserine [20], a phospholipid shown to be enriched on EV. Indeed, masking phosphatidylserine with annexin-V decreased EV uptake in vitro [21].

Herein, we describe approaches to overcome obstacles of EV production and delivery, which will facilitate further development of this therapeutic platform. We compare EV production using an efficient hollow-fiber culture system to that of conventional culture methods. We show that this method produces bioactive EV retaining surface proteins and can be used for the production of bioactive, EV associated heterodimeric interleukin-15. We also identify SR-A as a major receptor for the clearance of EV by monocyte/macrophages, and assess the applicability of SR-A blockade to achieve tumor delivery of administered EV in mice.

2. Materials and methods

2.1. Cells

HEK293 and all mouse cell lines (RAW264.7, 4T1, B16, LLC1, MC38 and EG.7) were obtained from ATCC. HEK293 cells expressing high levels of hetIL-15 were previously described [22,23]. NK92 cells were kindly provided by Dr. Howard A. Young (Cancer and Inflammation Program, National Cancer Institute, USA). Blood samples from healthy blood donors were collected in acid-citrate-dextrose tubes, under approved protocols for human subjects' research by the National Cancer Institute Investigational Review Board. Peripheral blood mononuclear cells (PBMC) were purified by gradient centrifugation over Histopaque-1077 (Sigma-Aldrich), according to the manufacturer's protocol.

4T1 cells were cultured in RPMI 1640 medium supplemented with 10% fetal calf serum. RAW264.7 and E.G7 cells were cultured in RPMI 1640 medium, supplemented with 5% fetal calf serum. The remaining cell lines were cultured in DMEM medium, supplemented with 10% fetal calf serum.

Human PBMC were cultured overnight in RPMI medium supplemented with 10% fetal calf serum and 100 U/mL penicillin/streptomycin. The cells were used within 24 h of purification from whole blood.

2.2. Cell culture method for EV production

EV/protein aggregate depleted cell culture medium was obtained by ultrafiltration of complete medium through a 500 kDa commercial hollow fiber ultrafiltration module (mPES MidiKros 500 kDa filter module, Spectrum Laboratories; Rancho Dominquez, CA), as previously described [14,24]. Specifically, a peristaltic pump was used to slowly circulate culture medium through the filter module, and filtrate was collected to be used as EV/protein aggregate depleted medium. The entire procedure was carried out using

sterile materials within a biosafety cabinet. Ultrafiltered supernatant was filtered a second time through a 0.22 μm filter device to ensure sterility.

To obtain conditioned medium from conventional cultures, 3 million cells were seeded in 175 cm^2 tissue culture flasks in DMEM supplemented with 10% fetal calf serum and 100 U/mL penicillin/streptomycin. After overnight incubation, cell monolayer was gently washed with PBS, and 15 mL of fresh EV/protein aggregate-depleted medium was added to each flask. 48 h later, conditioned medium was harvested and pooled for immediate EV purification. After conditioned medium was removed, cells were collected in PBS and pelleted by centrifugation at 300 × g. Cell lysates were prepared by addition of N1 lysis buffer to cell pellet, incubation on ice for 1 h, and two rounds of sonication for 6 s.

2.3. Fibercell hollow-fiber bioreactor culture

The HEK293 cell clone stably expressing hetIL-15 (clone 19.7) was expanded in conventional culture flasks and used to seed a medium-sized, hollow-fiber culture cartridge, with a 20 kDa molecular weight cut-off (Fibercell Systems; Frederick, MD). Cells were adapted over two weeks to bioreactor culture conditions by gradually increasing the proportion of protein-free medium (DMEM + 10% Fibercell Systems CDMHD protein-free supplement + 100 U/mL penicillin/streptomycin). Bioreactor conditioned medium (20 mL) was collected for each harvest three times per week. Harvests were cleared of cells by 300 × g centrifugation, and supernatants stored at −80 °C for further purification.

2.4. EV purification

After removing large cell debris by centrifugation at 3000 × g for 15 min, the supernatants were carefully moved to polycarbonate tubes, and spun for 45 min at 20,000 × g in a type 45Ti rotor (Beckman-Coulter; Brea, CA). Supernatants were then filtered through 0.22 μm Stericup device (EMD Millipore; Billerica, MA), moved to Snakeskin 10 kDa MWCO dialysis tubing (Thermo-Scientific; Grand Island, NY), and dialyzed overnight in >30 volumes of Tris-buffered saline (TBS). Dialyzed supernatants were centrifuged for 2 h at 110,000 × g in a type 70.1Ti rotor (Beckman-Coulter) to pellet EV. Pellets were resuspended to the original volume in TBS, by passing through a 27G needle approximately 5 times (until aggregates were no longer visible), and centrifuged again at 110,000 × g to wash away contaminating soluble proteins. EV pellets were resuspended in 1/50 original volume of TBS following the procedure described above. Finally, EV were additionally cleared of residual aggregation by 3 min centrifugation at 20,000 × g in a microfuge, and the supernatants containing the EV were transferred to a clean Lobind protein tube (Eppendorf; Hauppauge, NY), and stored at −80 °C for downstream applications. All purification steps were conducted at 4 °C.

For experiments directly comparing conventional culture to bioreactor EV, conditioned cell culture media were concentrated by ultrafiltration (Centricon-70, 100 kDa MWCO; EMD Millipore) prior to 110,000 × g centrifugation. This allowed for a larger volume of conventional flask-derived supernatants to be pooled prior to ultracentrifugation. Furthermore, initial EV pellet was not washed, but rather immediately resuspended in 100 μL TBS. These protocol modifications were implemented to allow for sufficient EV yields from conventional flask supernatants for downstream comparison analyses.

2.5. Biophysical characterization and imaging

Nanoparticle tracking analysis (NTA) was performed on fresh

and freeze-thawed EV samples in triplicate using a Nanosight LM10 (Malvern Instruments; Malvern, United Kingdom) to estimate size distribution (hydrodynamic diameter), particle concentration, and effects of freeze-thawing (Fig. S1). Samples were diluted to 1–2 µg/mL in PBS, and 3 videos of 30 s were acquired for each triplicate. Dynamic light scattering (DLS) was performed on a nanoparticle analyzer SZ-100 (Horiba Scientific) at the same dilution.

For transmission electron microscopy (TEM) sample preparation and imaging, EV suspensions were fixed with 2% glutaraldehyde (Electron Microscopy Sciences, Cat#16020) and then adsorbed to formvar/carbon coated TEM copper grids (SPI, Cat#3420C-MB). Samples were then negative stained with 1% Uranyl Acetate (Electron Microscopy Sciences, Cat# 22400) for 10 s. The samples were evaluated on a JEOL 1011 transmission electron microscope at 80 kV, and digital images were acquired using AMT camera system.

2.6. EV protein composition determination

Purified EV preparations were monitored for protein content by the Bradford assay, using bovine gamma-globulin as a standard. Specifically, 5 µL of EV preparation was added to 250 µL Quickstart Bradford reagent (Bio-Rad; Hercules, CA), and incubated for 15 min at room temperature. Protein concentration was quantified by measuring absorbance at 595 nm on a microplate reader.

For Western blots, EV were lysed by adding $5\times$ RIPA buffer and incubating on ice for 45 min. Antibodies used to probe the blots included: αCD63 (System Biosciences; Mountain View, CA), αAlix (clone 3A9, LifeSpan Biosciences; Seattle, WA), αIL-15 (AF315, R&D Systems) and αIL-15Rα (AF247, R&D Systems). All blots were probed overnight at 4 °C.

Detection of EV-associated IL-15 was performed by flow cytometry using the ExoFlow kit (System Biosciences) according to manufacturer's protocol. Briefly, 9.1 µm streptavidin-coated magnetic beads were loaded with biotinylated anti-CD63 exosome capture antibody. Next, 100 µg of purified EV were incubated overnight at 4 °C with antibody-loaded beads in a rotating microtube holder. EV-loaded magnetic beads were then washed using a magnetic tube stand, and divided for staining with individual fluorophore-conjugated antibodies: FITC-lectin (provided in kit) and PE-conjugated anti-IL-15 (clone 34559; R&D Systems, Minneapolis, MN). Incubation with antibodies was for 2 h on ice, gently flicking the tube to resuspend beads every 30 min. Finally, unbound antibody was washed from beads using a magnetic tube stand, and EV-loaded beads were acquired on a flow cytometer (LSR-II; BD Biosciences, Franklin Lakes, New Jersey).

2.7. Comparative proteomics study

$5\times$ RIPA buffer was added to EV samples (~20 µg), and incubated for 30 min on ice to lyse EV. Samples were then mixed with LDS gel loading buffer and NuPAGE sample reducing agent (Invitrogen), heated at 96 °C for 10 min, then, loaded on a 4–12% NuPAGE gel (Invitrogen). After two hours of running at a constant voltage (100 V), the gel was stained with SimplyBlue Safestain (Invitrogen). Each gel lane was excised into 12 gel slices. The gel slices were in-gel digested individually with Trypsin (Promega) at 37 °C overnight. Each digested peptide sample was desalted by C_{18} ZipTip (Millipore), lyophilized and re-suspended in 0.1% formic acid for LC-MS analysis. Each sample (6 µL) was loaded on an Easy nLC II nano-capillary HPLC system (Thermo Scientific) with a C_{18} Nano Trap Column, (Acclaim PepMap100 C_{18}, 2 cm, nanoViper, Thermo Scientific) and an analytical column (Acclaim PepMap RSLC C_{18}, 15 cm, nanoViper, Thermo Scientific) connected with a stainless steel emitter, coupled online with a Q Exactive hybrid OrbiTrap mass spectrometer (Thermo Scientific) for RPLC-MS/MS analysis.

Peptides were eluted using a linear gradient of 2% mobile phase B (acetonitrile with 0.1% formic acid) to 42% mobile phase B within 70 min at a constant flow rate of 200 nL/min. The twelve most intense molecular ions in the MS scan were sequentially selected for high-energy collisional dissociation (HCD) using a normalized collision energy of 30%. The mass spectra were acquired at the mass range of m/z 300–2000. The Easy Nano Spray ion source (Thermo Scientific) capillary voltage and temperature were set at 1.7 kV and 275 °C, respectively. The dynamic exclusion function on the mass spectrometer was enabled during the MS_2 data acquisition. The MS data were searched against the UniProt *Homo sapiens* database downloaded from the European Bioinformatics Institute website (http://www.ebi.ac.uk/integr8, January, 2016) utilizing Proteome Discoverer 1.4 (Thermo Scientific). Up to two missed tryptic cleavage sites was allowed during the database search. Oxidation (+15.9949 Da) of methionyl residue was included as dynamic modifications. The data was searched with a precursor ion tolerance of 20 ppm and a fragment ion tolerance of 50 ppm. The peptide identifications are filtered through protein percolator with the cutoff of a false peptide discover rate (FDR) less than 1% for all peptide identified. "Strict Maximum Parsimony Principle" was applied during the data compiling.

For comparative analysis of bioreactor vs. flask EV, peak area of peptide mappings (grouped by corresponding gene) were considered. Data were normalized to total peak area, using a normalization factor of 1.15.

2.8. Bioactivity assay

NK92 cells used for the IL-15 bioactivity assay were cultured in RPMI 1640 medium supplemented with 10% fetal calf serum, 100 U/mL penicillin/streptomycin, 200 U/mL recombinant IL-2 (National Cancer Institute), and 10 ng/mL hetIL-15 (Admune Therapeutics, Danvers, MA). Cell density was adjusted three times a week to a concentration of $3-4 \times 10^5$ cells/ml.

Purified EV were mixed with an equal volume of lysis buffer (1% Triton-X 100/200 mM Tris-HCl, pH7.4) and lysed by five freeze/thaw cycles. The amount of EV-associated IL-15 was assessed by ELISA (Human IL-15 Quantikine ELISA kit; R&D Systems, Minneapolis, MN) according to the manufacturer's instructions.

The bioactivity of EV-associated hetIL-15 was assessed on the human NK-92 cell line, which responds to IL-15 treatment by proliferating in a dose-dependent manner. NK-92 cells were cultured overnight at a concentration of 4×10^5 cells/mL in cytokine-free media prior to assay use. 50 µL of cytokine-starved NK-92 cells (4×10^5 cells/mL) were seeded in each assay well of 96-well plates. hetIL-15 purified protein standard (Admune Therapeutics) and purified EV samples were used to prepare solutions containing 0.05–2 ng/mL IL-15 (measured as single chain content) in complete cell culture medium; 50 µL of each IL-15 protein or EV solution was then added to the corresponding cell culture wells. Equal amounts of EV lacking IL-15 were used as negative control. After 72 h incubation, 25 µL MTT labeling reagent (Roche, Indianapolis, IN) was added to each well, and plates incubated for 5 h at 37 °C. Next, 100 µL solubilization buffer (10% SDS in 0.01 M HCl; Roche) was added to each well, and plates incubated for 24 h at 37 °C. Optical density of samples was measured at 570/690 nm, using a SpectraMax Plus 384 microplate reader (Molecular Devices, Sunnyvale, CA).

2.9. EV labeling for in vitro and in vivo tracking

Two different labeling dyes were used to monitor EV uptake: a green RNA dye (Syto RNASelect Green; Invitrogen, Grand Island, NY), and a near-infrared lipid dye (DiOC18(7) or DiR; Invitrogen).

For Syto RNASelect Green staining, 100 μg EV in 100 μL TBS were incubated with the dye at a final concentration of 10 μM for 30 min at 37 °C. For DiR staining, 62.5 μg EV in 100 μL TBS were incubated with the dye at a final concentration of 100 ng per microgram of EV for 1 h at 37 °C. After incubation, unincorporated dye was removed by gel filtration using PBS-hydrated Exosome Spin Columns (3 kDa MWCO, Invitrogen) (See Supplementary Fig. S7).

We also checked the stability of DiR staining of EV over 24 h (Fig. S8). DiR-stained EV were prepared as above, and incubated for 24 h at 37 °C. We then repeated the gel filtration procedure to remove any dye that may have become unincorporated from EV during the 24 h incubation. For comparison, we prepared freshly stained EV as above, and immediately performed a second gel filtration to account for EV losses in the Exosome Spin Columns. Stained EV from these samples were diluted 1:2, and 60 μL loaded in each well of a black-walled 96-well plate. Fluorescence intensity analysis of samples was performed in triplicate using the Odyssey Classic infrared imaging system (Li-Cor, Lincoln, NE) at the 800 nm channel.

2.10. In vitro SR-A blockade and EV uptake assessment

For EV uptake blocking experiments, mouse cells were first plated at a density of 250,000 cells per well in a 12-well plate and cultured overnight. E.G7 is a suspension cell line and 250,000 cells were used for each experimental sample. Cells were pre-treated for 30 min with fresh RPMI supplemented with 5% fetal calf serum medium, containing 100 μg/mL chondroitin sulfate, 100 μg/mL dextran sulfate or 10 μM BLT-1 (all EV-uptake blocking reagents obtained from Sigma-Aldrich, St. Louis, MO). Cells were washed once and incubated with fluorescently labeled EV for 2 h. The cells were harvested, washed, and resuspended in PBS+2% bovine serum albumin for the analysis of EV uptake by flow cytometry. The EV concentrations used in these experiments were adjusted to obtain 2—4 fold increase in the fluorescent signal above the auto-fluorescence from untreated cells (RAW 3.2 μg/mL; 4T1, MC38 and EG7: 1.6 μg/mL; LLC1 and B16: 0.8 μg/ml).

PBMC were cultured at 2×10^6 cells/mL and pretreated for 30 min with 500 μg/mL dextran sulfate, 500 μg/mL chondroitin sulfate, or left untreated. After washing, the cells were resuspended at a density of 4×10^6 cells/mL and incubated for 2 h with Syto RNASelect Green-labeled EV at a final concentration of 800 ng EV per mL, in a final volume of 0.5 mL. Finally, the cells were washed in PBS+0.2% AB+ human serum and stained with fluorophore-conjugated antibodies before flow cytometric analysis.

The following antibodies were used: αCD3-APC-Cy7 (clone SK7; BD Biosciences), αCD4-V500 (clone RPA-T4; BD Biosciences), αCD8-Alexa Fluor 405 (clone 3B5, Invitrogen), αCD14-PE (clone M5E2; BD Biosciences), αCD14-BV421 (clone HCD14; Biolegend; San Diego, CA), αCD19-Alexa Fluor 700 (clone HIB19; BD Biosciences), αCD56-APC (clone B159; BD Biosciences), and αCD204-PE (clone REA460; Miltenyi Biotec; San Diego, CA).

2.11. In vivo EV biodistribution in tumor-free and tumor-bearing mice after SR-A blockade

All animal experiments were conducted in compliance with the guidelines for the care and use of research animals established by the Animal Studies Committee of the National Institutes of Health. FVB or Balb/c mice were treated with the SR-A inhibitor dextran sulfate or chondroitin sulfate (negative control) at a dose of 30 mg/kg delivered in 100 μL PBS by tail vein injection. Control mice received 100 μL of PBS intraperitoneally. Two hours later, the mice received 100 μL of PBS containing 15 μg of DiR stained EV via the tail

vein. Imaging of live mice was performed at various time points, between 1 and 24 h post injection. Some mice were euthanized at different time points and their organs imaged ex vivo. Imaging was done on a Maestro™ 2 imaging system (Perkin Elmer).

For tumor inoculation studies, 1×10^6 4T1 cells in 100 μL of serum-free medium were implanted subcutaneously on the right front flank of female BALB/c mice. Once the tumor size reached a volume of 90—100 mm³, the animals were used for in vivo imaging experiments.

2.12. Statistical analyses

EV preparation purity and monocyte uptake of EV in vitro were analyzed using t-tests. EV preparation yield, along with liver, plasma, and tumor uptake (imaged ex vivo) were analyzed by 1-way ANOVA. Time courses of in vivo EV uptake by tumor and liver were analyzed with 2-way ANOVA. All statistical analyses were performed in Prism 6 (GraphPad Software, La Jolla, CA).

3. Results

3.1. High-yield EV production from hollow fiber bioreactor

In an effort to increase production yield, we used a lab-scale hollow-fiber bioreactor with protein-free culture medium to obtain conditioned cell culture supernatants as a source of EV. Hollow-fiber culture systems can sustain large numbers ($>10^9$) of cells, and produce highly concentrated cell culture supernatants from a variety of cells, including primary human cells [25,26]. We hypothesized that these characteristics would facilitate high-yield production and purification of EV.

HEK293 cells were adapted for growth in a hollow-fiber bioreactor using serum-free medium (Fig. 1A). EV from bioreactor or conventional tissue culture flask supernatants were purified by differential centrifugation, and the protein concentration of the purified materials was determined using the Bradford assay. Using a similar protocol of EV purification, bioreactor-harvested conditioned media yielded approximately 5-fold more EV compared to conventional flasks (Fig. 1B). Further optimization of the EV purification method, by omitting the supernatant concentration step, increased the EV yield about two-fold, resulting in a total 10× improved EV yield from cell culture conditioned media (Fig. 1B). NTA was used to estimate the particle to protein amount ratio, an indicator of EV purity [7,27]. We found a ratio of 1.09×10^9 ($\pm 2 \times 10^8$ particles)/μg of protein in EV preparations from the bioreactor, which is ~4-fold greater than the purity of preparations from our conventional cell culture (Fig. 1C), higher than has previously been reported for EV obtained from HEK293 cells [7]. EV markers CD63 and Alix were also enriched in preparations from bioreactor harvests, supporting increased purity (Fig. 1D). DLS (see Supplementary Fig. S2) and NTA (Fig. 2A), showed the majority of purified EV to be between 40 and 200 nm in diameter. TEM showed well-defined particles of comparable size (Fig. 2b). Together these data suggest that the use of hollow-fiber bioreactor, serum-free media and an optimized purification protocol represent a superior method to achieve high yield of purified EV (yields were >3 mg/week from a single lab-scale culture cartridge).

3.2. Comparison of bioreactor to flask-derived EV characteristics

We observed that the relative enrichment of CD63, as detected by Western blot (Fig. 1D), could not be fully accounted for by the increased particle purity of the bioreactor EV preparations. We therefore conducted an in-depth comparison of the particles purified from either source to assess whether the bioreactor
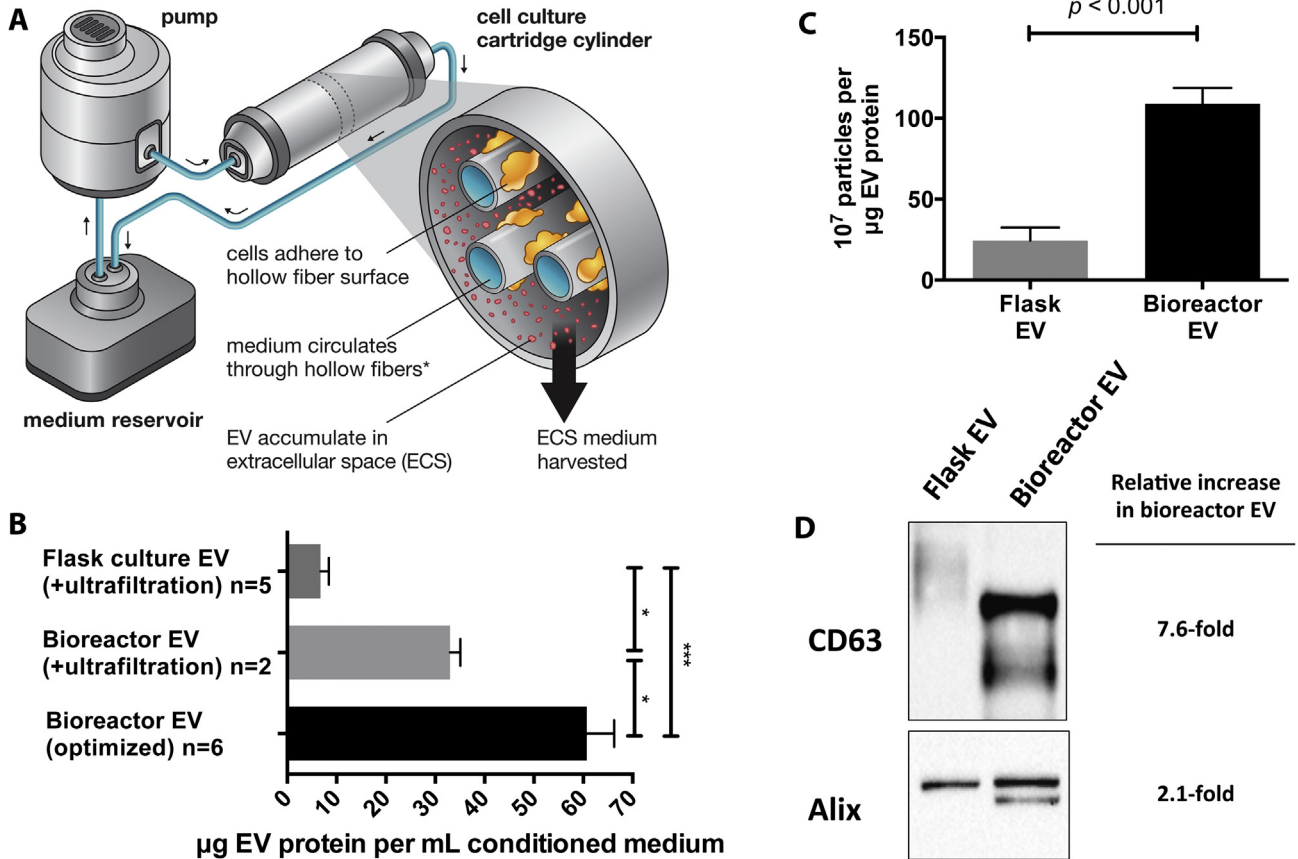
Fig. 1. Hollow-fiber bioreactor is a high-yield source of EV. (**A**) Schematic representation of EV production in hollow-fiber bioreactor. Fresh medium is pumped through the cell culture cartridge cylinder. Medium circulates within the hollow fibers of the culture cartridge, and (*) nutrient/waste exchange occurs through the hollow-fiber wall pores (20 kDa MWCO). Larger molecular weight cellular products (including EV) accumulate within the extracellular space of the cell culture cartridge cylinder. The extracellular space medium containing large amounts of EV is harvested every 1—3 days. (**B**) Yield of EV preparations from a hollow fiber bioreactor is ~10-fold more than conventional flask conditioned media. EV were purified from bioreactor conditioned media either by an optimized protocol (filtration, dialysis, and differential centrifugation) or by a protocol for direct comparison to conventional flask culture (ultrafiltration to concentrate conditioned media, filtration, and differential centrifugation). Protein yield, calculated as μg EV-associated protein per milliliter original conditioned medium (mean ± SEM), was quantified in independent preparations, and compared by ANOVA (*p < 0.05; ***p < 0.001). (**C**) Particle purity of EV preparations from a hollow fiber bioreactor is ~4-fold higher than conventional flask conditioned media. Particle purity indicates the level of EV-free protein contamination of EV preparations, and was assessed as the number of particles per μg protein, as measured by nanoparticle tracking analysis. (**D**) Enrichment of EV-associated markers in western blot of bioreactor EV preparations vs. conventional flask culture suggests higher purity. Each lane was loaded with 20 μg total protein, and band intensity quantification was performed by densitometry. In bioreactor EV preparations, we also observed differentially processed forms of associated proteins. In the case of CD63, lower molecular weight bands may reflect differential glycosylation pattern, as this protein has several glycosylation modifications. For Alix, there are several known phosphorylation sites, whose differential status could explain the second band. Detection of differentially processed proteins may be the result of increased amount of the EV markers and/or altered biocomposition of EV produced by cells grown under different bioreactor conditions.
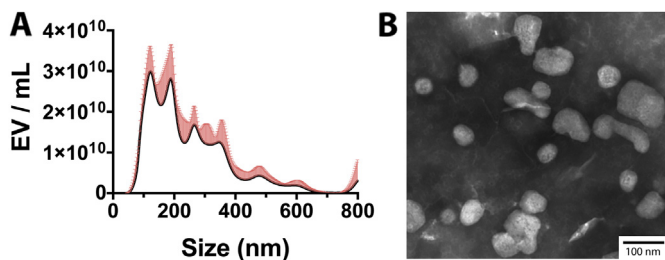

Fig. 2. Biophysical characterization of purified bioreactor EV. (**A**) Nanoparticle tracking analysis (NTA) was used to characterize the size of purified EV, as shown in representative size frequency distribution plot. Each sample for was run in triplicate at 1—2 μg/mL concentration. Black line represents mean values, and red shaded area represents SEM. NTA was able to distinguish three main subpopulations based on size corresponding to peaks of approximately 120, 190, and 280 nm in diameter. (**B**) Transmission electron micrograph of bioreactor EV.

methodology changes the profile of purified EV. A side-by-side comparison of NTA plots from several preparations of EV from either method revealed that the size distribution of culture-flask derived EV was more limited (Fig. S3), which could be a result of a different mixture of EV subpopulations. Serum-free culture conditions have previously been reported to affect EV composition [28], so we further compared the composition of bioreactor vs. flask EV by comparative proteomics, using mass spectrometry (Supplementary File 1 and Fig. S4). Many proteins were shared between the two samples, including EV markers such as CD63, Alix, and TSG101. However, serum proteins were over-represented in the flask EV.

3.3. Purified bioreactor EV are bioactive in vitro

We used a HEK293 cell clone that expresses the human membrane-associated heterodimeric interleukin-15 complex, IL-15:IL-15Rα (hetIL-15) [22,23], to examine whether optimally purified EV maintain functional hetIL-15 on their surface (Fig. 3A).

Given its function as an expander and activator of natural killer and cytotoxic T-cells [23], IL-15 is being developed as a potential cancer immunotherapeutic in clinical studies [29]. The presence of EV-associated hetIL-15 was confirmed by Western blot using antibodies against the two polypeptide chains of hetIL-15, IL-15 and IL-15Rα (Fig. 3B). Upon surface expression, the full length ~59 kDa IL-15Rα is cleaved and secreted as a soluble ~42 kDa molecule [23]. Indeed, EV-associated IL-15Rα was mostly of the larger membrane-associated species, which was also detected in association with cell lysates (Fig. 3C). Flow cytometric analysis verified that hetIL-15 was associated with the EV surface (Fig. 3D). The bioactivity of EV-associated hetIL-15 was confirmed *in vitro* by using an established MTT-based proliferation assay on the human NK-92 cell line. Upon stimulation by either form of the cytokine (soluble or EV-associated), NK-92 cells proliferated to a similar degree (Fig. 3E), indicating that purified EV maintain bioactive properties.

3.4. Scavenger receptor A family (SR-A) mediates EV binding to monocytes/macrophages

We assessed the contribution of SR-A to EV uptake *in vitro* by using dextran sulfate, a molecule known to block this receptor [30,31]. Chondroitin sulfate was used as a control for any non-specific activity of dextran sulfate [30,31], as both molecules are negatively charged carbohydrate polymers. By flow cytometry, we confirmed that the murine macrophage cell line RAW 264.7 expresses the SR-A1 receptor isoform, while a panel of tumor cell lines lacks the expression of this receptor (see Supplementary Fig. S5). In agreement with the SR-A1 expression levels, dextran pre-treatment of RAW 264.7 cells resulted in a 30—50% decrease in EV uptake when incubated with fluorescently-labeled EV, whereas this effect was not observed in the tumor cell lines that lacked SR-A1 expression (Fig. 4A). Given the contemporaneous report of BLT-1

(a known SR-B1 blocker) blocking EV uptake in macrophages [32], we combined this molecule with dextran sulfate in the RAW 264.7 cell assay, and found an additive effect of dual scavenger receptor blockade (Fig. S6).

We also addressed the contribution of SR-A on EV uptake by human peripheral blood mononuclear cells (PBMC), a heterogeneous population of primary human cells. PBMC, pretreated with dextran sulfate, were exposed to labeled EV, and EV uptake in different primary cell subsets was monitored by flow cytometry, using a combination of fluorescently labeled monoclonal antibodies. These experiments demonstrated that most EV were bound to monocytes and that 30—60% of this uptake could be abrogated by SR-A blocking (Fig. 4B).

3.5. SR-A blockade changes biodistribution of administered EV

We tested the hypothesis that blocking SR-A receptors would impact EV biodistribution by treating mice pretreated with either dextran sulfate or chondroitin with DiR-labeled EV by tail vein injection. EV biodistribution was monitored by fluorescence imaging of live mice as well as excised organs. Imaging performed at 2 h post-injection of EV showed that SR-A blockade decreased liver uptake of EV by ~50% (Fig. 5). In contrast, SR-A blockade by dextran sulfate significantly increased the amount of EV circulating in the plasma (Fig. 5). Thus, blocking the EV receptor SR-A led to significant changes in EV biodistribution.

3.6. Tumor accumulation of administered EV is enabled by SR-A blockade

Next, we assessed whether blocking monocyte/macrophage uptake results in enhanced tumor accumulation of EV, in the absence of targeting ligands. Immunocompetent mice bearing
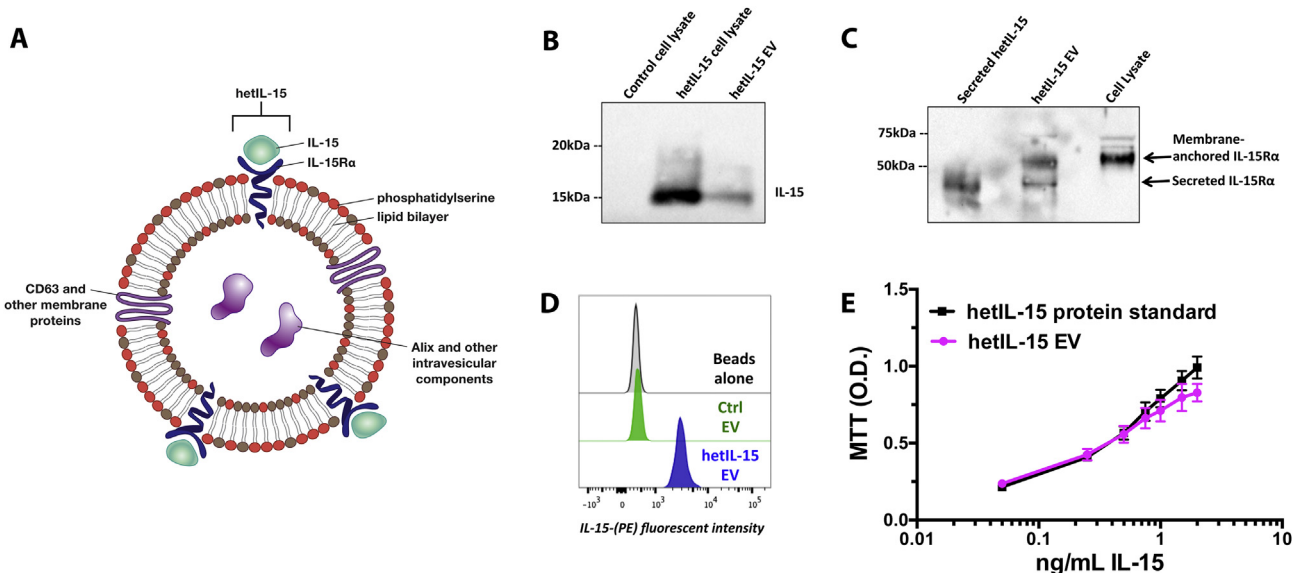

Fig. 3. EV purified from hollow fiber bioreactor and containing surface hetIL-15 retain IL-15 bioactivity. (**A**) Schematic representation of EV bearing hetIL-15. (**B**) Western blot shows the presence of IL-15 cytokine in cell lysate and in bioreactor-derived EV from a HEK293 cell clone that stably overexpresses the IL-15 heterodimer complex (IL-15:IL-15Rα). Control cell lysate is from parental HEK293 cell line. (**C**) EV-associated IL-15Rα is primarily membrane anchored. Western blot of IL-15Rα associated with bioreactor EV preparation. The apparent molecular weight of the EV-associated protein was compared to that detected in the cell lysate (transmembrane protein) and in purified secreted hetIL-15 (truncated, secreted protein). The majority of EV-associated IL-15Rα is the same size as that of the cell-associated (membrane-anchored) cytokine. (**D**) EV-associated hetIL-15 is displayed on vesicular surface. Flow cytometry histograms show signal intensity from EV probed with PE-conjugated αIL-15 antibody. EV were first captured on αCD63 antibody-coated beads and probed with fluorophore-conjugated antibody to detect presence of surface cytokine. Control EV were derived from parental HEK293 cells and hetIL-15 EV came from a HEK293 cell clone stably overexpressing the cytokine. (**E**) EV-associated IL-15 is bioactive *in vitro*. Bioactivity assessed as proliferation of the NK92 cell line following 72 h incubation, as quantified by mean MTT assay O.D in 6 wells per sample (mean ± SEM). Magenta line represents bioactivity of 3 independent EV preparations from bioreactor supernatants of a HEK293 cell clone overexpressing hetIL-15. Black line represents triplicate bioactivity assessment of protein standard. Incubation of cells with equal protein amount of control HEK293 cell EV resulted in MTT O.D. <0.25.
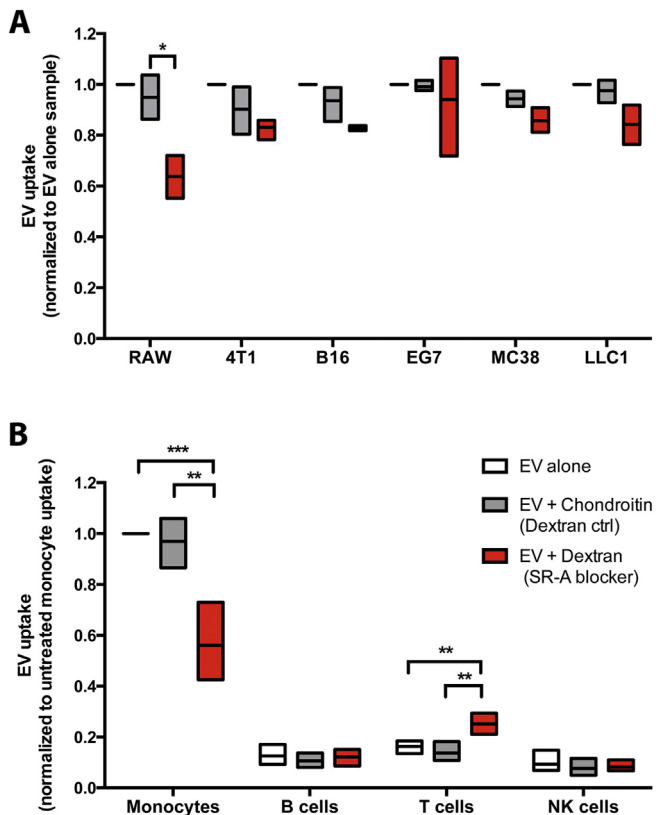
Fig. 4. EV uptake in monocytes/macrophages is largely mediated by the Scavenger receptor A family (SR-A). Cells were pretreated with dextran sulfate (SR-A blocker) or chondroitin sulfate (dextran control) for 30 min. After washing away inhibitor, stained EV were added for 2 h. Flow cytometry was used to quantify EV uptake by fluorescent intensity of cells. Boxes represent range of values (min to max), and line in box denotes group mean. Uptake compared between groups by multiple t-tests, with Holm-Sidak correction for multiple comparisons (Cumulative alpha-error <0.05). One (*), two (**), and three (***) asterisks denote $p < 0.05$, $p < 0.01$, and $p < 0.001$, respectively. (**A**) Blocking SR-A with dextran sulfate decreased EV uptake by 30–50% only in RAW cells, and not in cell lines that lack SR-A expression (in three independent experiments). Viability of cells assessed by Live/Dead fluorescent stain (Invitrogen) showed no effect of treatment conditions in the tested cell lines (data not shown). (**B**) Monocytes uptake the majority of EV among primary human PBMC cultured *in vitro*, through SR-A (n = 4). EV uptake was quantified by mean fluorescent intensity above background, and normalized to EV uptake by untreated monocytes of each donor sample.

subcutaneous 4T1 breast cancer cell tumors were pretreated with the SR-A blocker, followed by systemic delivery of labeled EV. Imaging of live mice over a period of 24 h showed that significant intratumoral EV accumulation could only be observed in animals pretreated with dextran sulfate (Figs. 6 and 7), even though SR-A blockade of the liver diminished over 24 h (Fig. 6C, right panel). *Ex vivo* measurements also showed that EV tumor uptake increased by ~3-fold over the 24-h period (Fig. 7).

4. Discussion

In this study, we developed methods for the purification of bioactive EV, carrying membrane-embedded heterodimeric IL-15. These results indicate the presence of a third form of heterodimeric IL-15 in addition to the soluble and the cell membrane-embedded forms [22,23,33,34]. Presence of functional hetIL-15 on EV may have significant physiologic roles and implications. It was previously shown that IL-15 Receptor alpha (the stabilizing component of hetIL-15) is expressed on EV from cultured human dendritic cells, which can directly activate NK cells only in the

presence of exogenous recombinant IL-15 (active cytokine component of hetIL-15) [35]. Contrarily, EV purified from HEK293 cells expressing hetIL-15 maintain IL-15 bioactivity without addition of exogenous cytokine, which could be a significant benefit when using EV as therapeutics. Furthermore, it remains to be examined whether primary human dendritic cells also secrete functionally significant EV bearing complete hetIL-15 under conditions not tested previously (e.g. stimulation by certain toll-like receptor ligands) [36].

We developed a methodology for the mass production of highly purified, bioactive EV using a lab-scale hollow fiber bioreactor, which may facilitate further *in vivo* studies. This method presents many advantages over conventional culture that likely contribute to the higher EV production yield and purity that we observed. First, lab-scale hollow fiber bioreactors enable the sustained maintenance of large numbers of cells (estimated by the manufacturer to be in the order of 10^9 cells) within a standard incubator, with minimal maintenance. Specifically, a 2 L bottle of medium is simply replaced every 2 days. More importantly, all of the cultured cells secrete EV into the relatively small volume of the culture cartridge extracapillary space (~60 mL) resulting in EV-rich conditioned medium that can be used directly for EV purification. Our findings suggest that this method yields 40-fold more EV particles per volume of conditioned medium vs. conventional cell culture. Thus, to match a single daily harvest of the hollow-fiber bioreactor (20 mL), an estimated 53 large (175 cm^2) flasks producing 800 mL conditioned medium would be required. Moreover, cells grown in hollow-fiber bioreactors readily adapt to sustained growth in protein-free medium, which also facilitates EV purification without serum contaminants, as highlighted by our comparative proteomics study. On the other hand, bioreactor EV preparations may have a more diverse population of EV, as suggested by the increased size range. Thus, further purification of preparations (e.g. by density gradient) may be required for some applications.

Our findings showing the greatly enhanced yield of EV purified from hollow-fiber cultures may also have significant implications for the development of clinical grade EV therapeutics, given that hollow-fiber methods have already been used to expand primary human cells under cGMP conditions [25,26].

Moreover, we show for the first time that blocking SR-A, a novel receptor for EV, enables accumulation of even untargeted EV in several tissues, including tumors (Fig. 8). Our *in vitro* findings showed that monocytes/macrophages are uniquely affected by SR-A blockade with respect to EV uptake. Interestingly, in the mixed PBMC culture, the blockade of monocyte EV uptake was accompanied by an increase in uptake by T-cells, perhaps a result of EV binding to a different receptor on the latter. *In vivo*, increased circulation and accumulation within tumors coincided with decreased liver uptake, confirming previous findings that liver macrophages rapidly clear administered EV in the absence of scavenger receptor blockade [17]. When chondroitin sulfate or dextran sulfate were administered to mice prior to labeled EV injection, we observed an increase in splenic uptake of EV compared to mice receiving EV alone (Fig. 5). A possible explanation for this could be the trafficking of circulating monocytes to the spleen after uptake of either negatively charged polymer, as has been described previously for negatively charged poly(lactic-co-glycolic acid) (PLGA) formulations [37]. At the highest dose of dextran, even though monocytes are still possibly sequestered in the spleen, their EV uptake capacity would be largely inhibited, resulting in the lower splenic EV uptake of this group. In any case, SR-A blockade by dextran sulfate consistently decreased liver uptake of EV, and significantly increased their ability to accumulate within tumors.

Considering the massive EV clearance by the RES under physiological conditions, our results are important for EV therapeutic
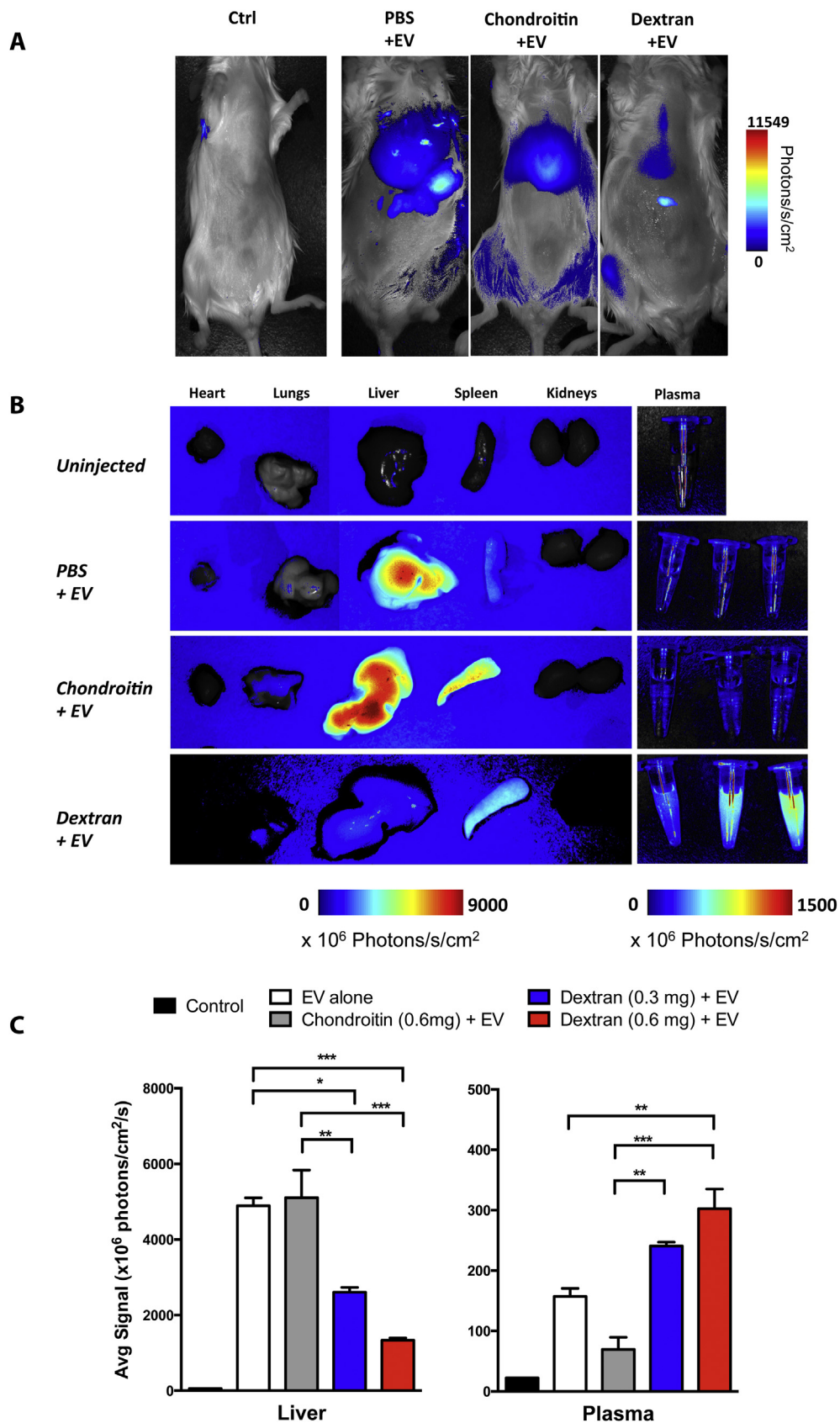
Fig. 5. SR-A blockade decreases liver clearance of EV. FVB mice were pre-treated with 0.6 mg dextran sulfate, chondroitin sulfate, or PBS. 15 µg DiR-stained EV were then injected intravenously and mice were imaged 2 h later. (**A**) Live animal imaging showing dramatically decreased liver uptake of EV with SR-A blocker pre-treatment. (**B**) Organ bio-distribution of administered EV changes after SR-A blockade. A representative image of excised organs is shown from each group. Plasma is shown from three different mice of each group. (**C**) Quantitation of EV accumulation in excised organs showed decrease of liver uptake, and increase in circulating EV at 2 h in the mice receiving dextran sulfate. Bars represent group mean + SEM (n = 3). Uptake was compared between groups using ANOVA, with Turkey correction for multiple comparisons. One (*), two (**), and three (***) asterisks denote $p < 0.05$, $p < 0.01$, and $p < 0.001$, respectively.
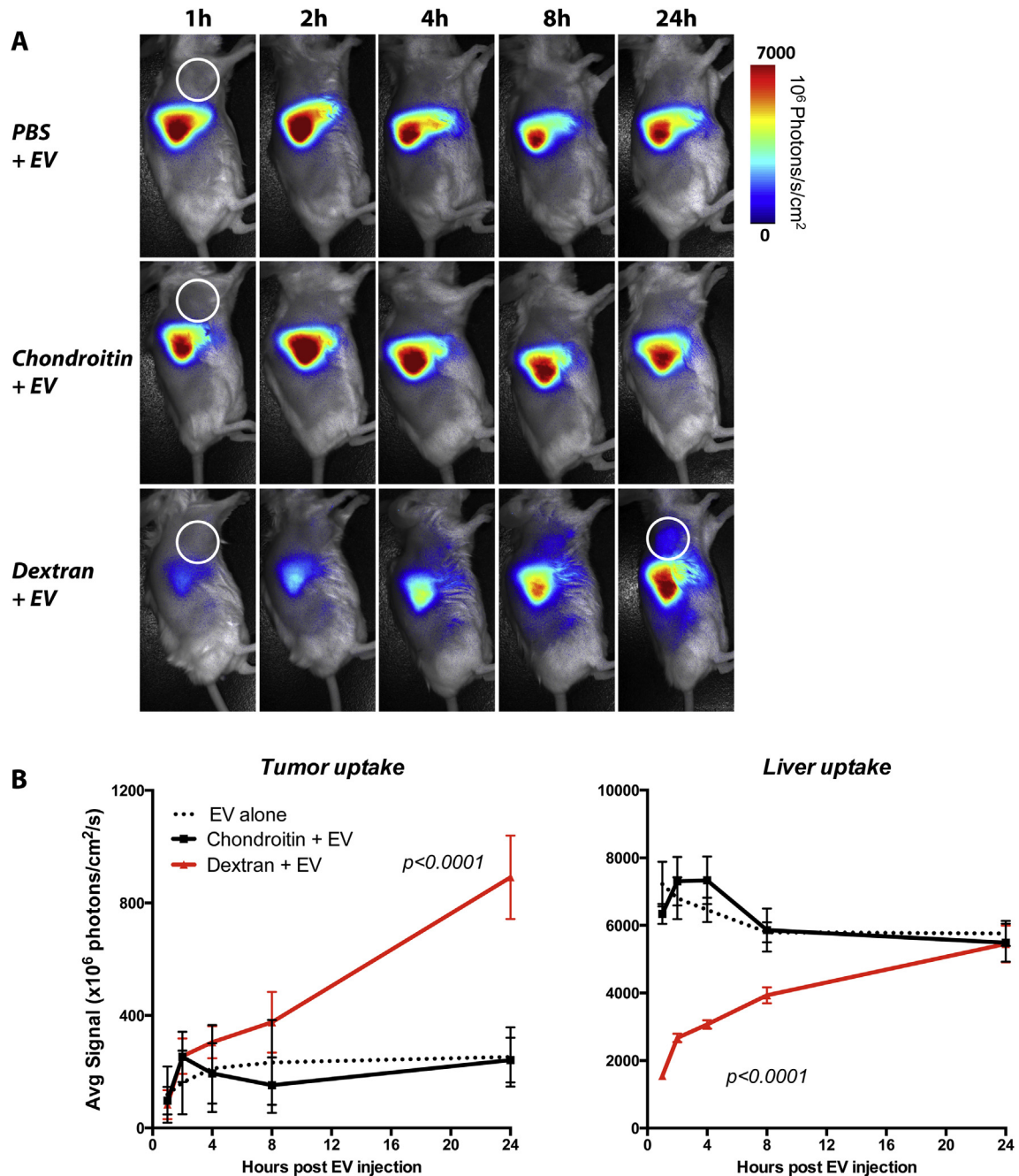
Fig. 6. Kinetics of EV uptake by liver and tumor following single injection of SR-A blocker in subcutaneous 4T1 tumor-bearing Balb/c mice (tumor location indicated by white circle). Mice were pretreated with either PBS, 0.6 mg dextran or chondroitin, injected IV with 15 μg stained EV, and imaged live at the indicated time points. (**A**) Serial live animal imaging showing early inhibition of EV uptake by the liver, and gradual accumulation of EV in the tumor only in mice pre-treated with the SR-A blocker dextran sulfate. (**B**) Time course of EV uptake (mean ± SEM) in tumor and liver of 4T1 bearing Balb/c mice (n = 4 per group), analyzed by 2-way ANOVA. Tumor accumulation increases significantly with time in SR-A blocked mice (left panel), even though liver uptake blockade was transient, following a single injection of dextran sulfate (right panel).

applications. Our findings make the case for developing potent SR-A blockers with favorable toxicity profiles. Combining scavenger receptor blockade with EV targeting using relevant ligands may further improve the targeted delivery of therapeutic RNA, viral vectors or any other molecules. Given that small molecules and peptides with the potential to block SR-A and other scavenger receptors are under development and some are in clinical trials [38—40], blocking RES uptake in therapeutic settings comprises a promising approach to enable a broad spectrum of effective EV-based therapeutics.

Author contributions

D.C.W., D.B., A.S., C.B., A.V., J.B., M.M., M.S., A.M.K., and J.C.J. conducted experiments. G.N., B.K.F., X.C., I.G., and G.N.P. supervised research. D.C.W., D.B., A.S., and G.N.P. wrote and edited the manuscript.

Conflict of interest

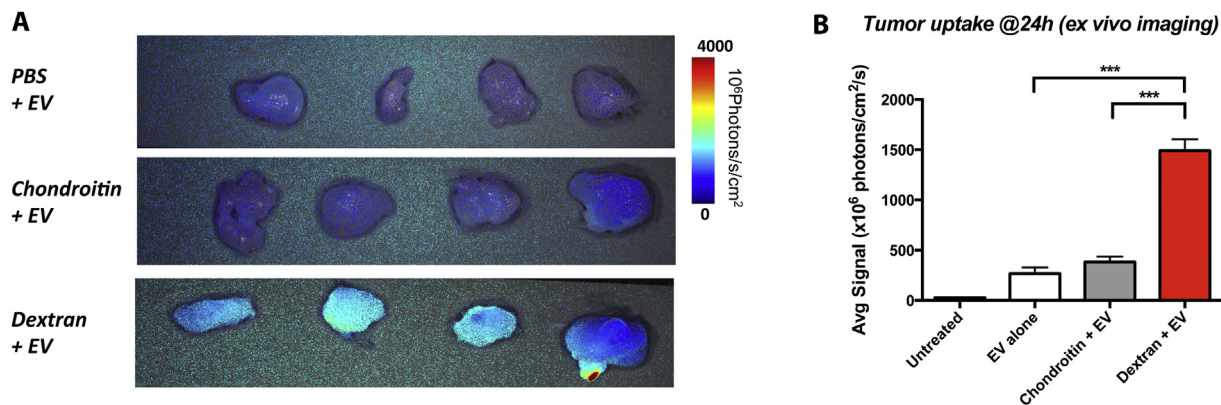The authors declare no competing financial interest.

Fig. 7. Significant EV uptake detected at 24 h in excised 4T1 tumors only from mice pre-treated with the SR-A blocker dextran sulfate. Mice were pretreated with either PBS, 0.6 mg dextran or chondroitin, and injected IV with 15 μg stained EV. (**A**) Fluorescence imaging of excised tumors showing increased EV uptake in dextran-pretreated mice. (**B**) Quantitation of EV accumulation in excised tumors of SR-A blocked mice, after 24 h. Bars display group mean ± SEM. Uptake compared between groups by ANOVA, with Sidak correction for multiple comparisons. Three asterisks (***) denote $p < 0.001$.
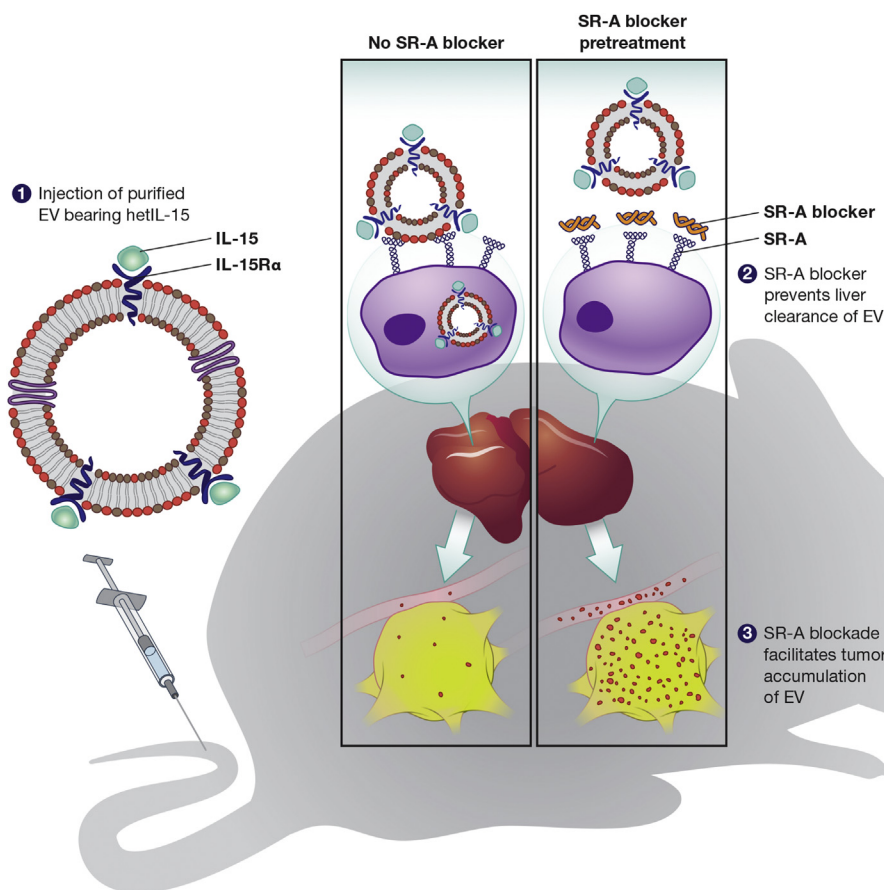

Fig. 8. Schematic depiction of the application of SR-A blockade for tumor delivery of EV carrying therapeutic molecules.

Acknowledgments

Appendix A. Supplementary data

Supplementary data related to this article can be found at http://dx.doi.org/10.1016/j.biomaterials.2016.07.003.

References

[1] L. Zitvogel, A. Regnault, A. Lozier, J. Wolfers, C. Flament, D. Tenza, P. Ricciardi-

Castagnoli, G. Raposo, S. Amigorena, Eradication of established murine tumors using a novel cell-free vaccine: dendritic cell-derived exosomes, Nat. Med. 4 (5) (1998) 594—600.

[2] S.H. Kim, N.R. Bianco, W.J. Shufesky, A.E. Morelli, P.D. Robbins, MHC class II+ exosomes in plasma suppress inflammation in an antigen-specific and Fas ligand/Fas-dependent manner, J. Immunol. 179 (4) (2007) 2235—2241.

[3] L. Alvarez-Erviti, Y. Seow, H. Yin, C. Betts, S. Lakhal, M.J. Wood, Delivery of siRNA to the mouse brain by systemic injection of targeted exosomes, Nat. Biotechnol. 29 (4) (2011) 341—345.

[4] O.P. Wiklander, J.Z. Nordin, A. O'Loughlin, Y. Gustafsson, G. Corso, I. Mager, P. Vader, Y. Lee, H. Sork, Y. Seow, N. Heldring, L. Alvarez-Erviti, C.E. Smith, K. Le Blanc, P. Macchiarini, P. Jungebluth, M.J. Wood, S.E. Andaloussi, Extracellular vesicle in vivo biodistribution is determined by cell source, route of administration and targeting, J. Extracell. Vesicles 4 (2015) 26316.

[5] M.J. Haney, N.L. Klyachko, Y. Zhao, R. Gupta, E.G. Plotnikova, Z. He, T. Patel, A. Piroyan, M. Sokolsky, A.V. Kabanov, E.V. Batrakova, Exosomes as drug delivery vehicles for Parkinson's disease therapy, J. Control Release 207 (2015) 18—30.

[6] R.B. Rountree, S.J. Mandl, J.M. Nachtwey, K. Dalpozzo, L. Do, J.R. Lombardo, P.L. Schoonmaker, K. Brinkmann, U. Dirmeier, R. Laus, A. Delcayre, Exosome targeting of tumor antigens expressed by cancer vaccines can improve antigen immunogenicity and therapeutic efficacy, Cancer Res. 71 (15) (2011) 5235—5244.

[7] S. El-Andaloussi, Y. Lee, S. Lakhal-Littleton, J. Li, Y. Seow, C. Gardiner, L. Alvarez-Erviti, I.L. Sargent, M.J. Wood, Exosome-mediated delivery of siRNA in vitro and in vivo, Nat. Protoc. 7 (12) (2012) 2112—2126.

[8] B. Gyorgy, Z. Fitzpatrick, M.H. Crommentuijn, D. Mu, C.A. Maguire, Naturally enveloped AAV vectors for shielding neutralizing antibodies and robust gene delivery in vivo, Biomaterials 35 (26) (2014) 7598—7609.

[9] G. Toffoli, M. Hadla, G. Corona, I. Caligiuri, S. Palazzolo, S. Semeraro, A. Gamini, V. Canzonieri, F. Rizzolio, Exosomal doxorubicin reduces the cardiac toxicity of doxorubicin, Nanomed. (Lond.) 10 (19) (2015) 2963—2971.

[10] C. Lasser, M. Eldh, J. Lotvall, Isolation and characterization of RNA-containing exosomes, J. Vis. Exp. 59 (2012) e3037.

[11] H. Shin, C. Han, J.M. Labuz, J. Kim, J. Kim, S. Cho, Y.S. Gho, S. Takayama, J. Park, High-yield isolation of extracellular vesicles using aqueous two-phase system, Sci. Rep. 5 (2015) 13103.

[12] D.W. Greening, R. Xu, H. Ji, B.J. Tauro, R.J. Simpson, A protocol for exosome isolation and characterization: evaluation of ultracentrifugation, density-gradient separation, and immunoaffinity capture methods, Methods Mol. Biol. 1295 (2015) 179—209.

[13] J.P. Mitchell, J. Court, M.D. Mason, Z. Tabi, A. Clayton, Increased exosome production from tumour cell cultures using the Integra CELLine Culture System, J. Immunol. Methods 335 (1—2) (2008) 98—105.

[14] H.G. Lamparski, A. Metha-Damani, J.-Y. Yao, S. Patel, D.-H. Hsu, C. Ruegg, J.-B. Le Pecq, Production and characterization of clinical grade exosomes derived from dendritic cells, J. Immunol. Methods 270 (2002) 211—226.

[15] S. Ohno, M. Takanashi, K. Sudo, S. Ueda, A. Ishikawa, N. Matsuyama, K. Fujita, T. Mizutani, T. Ohgi, T. Ochiya, N. Gotoh, M. Kuroda, Systemically injected exosomes targeted to EGFR deliver antitumor microRNA to breast cancer cells, Mol. Ther. 21 (1) (2013) 185—191.

[16] T. Smyth, M. Kullberg, N. Malik, P. Smith-Jones, M.W. Graner, T.J. Anchordoquy, Biodistribution and delivery efficiency of unmodified tumor-derived exosomes, J. Control Release 199 (2015) 145—155.

[17] T. Imai, Y. Takahashi, M. Nishikawa, K. Kato, M. Morishita, T. Yamashita, A. Matsumoto, C. Charoenviriyakul, Y. Takakura, Macrophage-dependent clearance of systemically administered B16BL6-derived exosomes from the blood circulation in mice, J. Extracell. Vesicles 4 (2015) 26238.

[18] S. Bala, T. Csak, F. Momen-Heravi, D. Lippai, K. Kodys, D. Catalano, A. Satishchandran, V. Ambros, G. Szabo, Biodistribution and function of extracellular miRNA-155 in mice, Sci. Rep. 5 (2015) 10721.

[19] M. Morishita, Y. Takahashi, M. Nishikawa, K. Sano, K. Kato, T. Yamashita, T. Imai, H. Saji, Y. Takakura, Quantitative analysis of tissue distribution of the B16BL6-derived exosomes using a streptavidin-lactadherin fusion protein and iodine-125-labeled biotin derivative after intravenous injection in mice, J. Pharm. Sci. 104 (2) (2015) 705—713.

[20] D.G. You, G. Saravanakumar, S. Son, H.S. Han, R. Heo, K. Kim, I.C. Kwon, J.Y. Lee, J.H. Park, Dextran sulfate-coated superparamagnetic iron oxide nanoparticles as a contrast agent for atherosclerosis imaging, Carbohydr. Polym. 101 (2014) 1225—1233.

[21] K. Yuyama, H. Sun, S. Mitsutake, Y. Igarashi, Sphingolipid-modulated exosome secretion promotes clearance of amyloid-beta by microglia, J. Biol. Chem. 287 (14) (2012) 10977—10989.

[22] E. Chertova, C. Bergamaschi, O. Chertov, R. Sowder, J. Bear, J.D. Roser, R.K. Beach, J.D. Lifson, B.K. Felber, G.N. Pavlakis, Characterization and favorable in vivo properties of heterodimeric soluble IL-15.IL-15Ralpha cytokine compared to IL-15 monomer, J. Biol. Chem. 288 (25) (2013) 18093—18103.

[23] C. Bergamaschi, M. Rosati, R. Jalah, A. Valentin, V. Kulkarni, C. Alicea,

G.M. Zhang, V. Patel, B.K. Felber, G.N. Pavlakis, Intracellular interaction of interleukin-15 with its receptor alpha during production leads to mutual stabilization and increased bioactivity, J. Biol. Chem. 283 (7) (2008) 4189—4199.

[24] M.L. Heinemann, M. Ilmer, L.P. Silva, D.H. Hawke, A. Recio, M.A. Vorontsova, E. Alt, J. Vykoukal, Benchtop isolation and characterization of functional exosomes by sequential filtration, J. Chromatogr. A 1371C (2014) 125—135.

[25] K. T.N. Startz, R. Peters, B. Nankervis, M. Jones, R. Kilian, N. Frank, B. Vang, D. Hill, Maturation of dendritic cells from CD14+ monocytes in an automated functionally closed hollow fiber bioreactor system, Cytotherapy 16 (4) (2014) S29.

[26] V. Boah, N. Frank, D. Hill, M. Domicina, M. Jones, B. Nankervis, R. Peters, T.P. Starz, K. Nguyen, Expansion of Adult Bone Marrow-derived Mesenchymal Stem Cells in the Quantum® Cell Expansion System Produces Therapeutic Doses under Hypoxic Conditions, International Society for Stem Cell Research Meeting, Boston, MA, 2013. Available at: https://www.terumobct.com/location/emea/products-and-services/Pages/Quantum-Materials.aspx.

[27] J. Webber, A. Clayton, How pure are your vesicles? J. Extracell. Vesicles 2 (2013).

[28] J. Li, Y. Lee, H.J. Johansson, I. Mager, P. Vader, J.Z. Nordin, O.P. Wiklander, J. Lehtio, M.J. Wood, S.E. Andaloussi, Serum-free culture alters the quantity and protein composition of neuroblastoma-derived extracellular vesicles, J. Extracell. Vesicles 4 (2015) 26883.

[29] K.C. Conlon, E. Lugli, H.C. Welles, S.A. Rosenberg, A.T. Fojo, J.C. Morris, T.A. Fleisher, S.P. Dubois, L.P. Perera, D.M. Stewart, C.K. Goldman, B.R. Bryant, J.M. Decker, J. Chen, T.A. Worthy, W.D. Figg Sr., C.J. Peer, M.C. Sneller, H.C. Lane, J.L. Yovandich, S.P. Creekmore, M. Roederer, T.A. Waldmann, Redistribution, hyperproliferation, activation of natural killer cells and CD8 T cells, and cytokine production during first-in-human clinical trial of recombinant human interleukin-15 in patients with cancer, J. Clin. Oncol. 33 (1) (2015) 74—82.

[30] T. Thelen, Y. Hao, A.I. Medeiros, J.L. Curtis, C.H. Serezani, L. Kobzik, L.H. Harris, D.M. Aronoff, The class A scavenger receptor, macrophage receptor with collagenous structure, is the major phagocytic receptor for Clostridium sordellii expressed by human decidual macrophages, J. Immunol. 185 (7) (2010) 4328—4335.

[31] G.V. Limmon, M. Arredouani, K.L. McCann, R.A. Corn Minor, L. Kobzik, F. Imani, Scavenger receptor class-A is a novel cell surface receptor for double-stranded RNA, FASEB J. 22 (1) (2008) 159—167.

[32] M.P. Plebanek, R.K. Mutharasan, O. Volpert, A. Matov, J.C. Gatlin, C.S. Thaxton, Nanoparticle targeting and cholesterol flux through scavenger receptor type B-1 inhibits cellular exosome uptake, Sci. Rep. 5 (2015) 15724.

[33] C. Bergamaschi, J. Bear, M. Rosati, R.K. Beach, C. Alicea, R. Sowder, E. Chertova, S.A. Rosenberg, B.K. Felber, G.N. Pavlakis, Circulating IL-15 exists as heterodimeric complex with soluble IL-15Ralpha in human and mouse serum, Blood 120 (1) (2012) e1—8.

[34] M. Thaysen-Andersen, E. Chertova, C. Bergamaschi, E.S. Moh, O. Chertov, J. Roser, R. Sowder, J. Bear, J. Lifson, N.H. Packer, B.K. Felber, G.N. Pavlakis, Recombinant human heterodimeric IL-15 complex displays extensive and reproducible N- and O-linked glycosylation, Glycoconj. J. 33 (3) (2016) 417—433.

[35] S. Viaud, M. Terme, C. Flament, J. Taieb, F. Andre, S. Novault, B. Escudier, C. Robert, S. Caillat-Zucman, T. Tursz, L. Zitvogel, N. Chaput, Dendritic cell-derived exosomes promote natural killer cell activation and proliferation: a role for NKG2D ligands and IL-15Ralpha, PLoS One 4 (3) (2009) e4942.

[36] E. Mortier, T. Woo, R. Advincula, S. Gozalo, A. Ma, IL-15Ralpha chaperones IL-15 to stable dendritic cell membrane complexes that activate NK cells via trans presentation, J. Exp. Med. 205 (5) (2008) 1213—1225.

[37] D.R. Getts, R.L. Terry, M.T. Getts, C. Deffrasnes, M. Muller, C. van Vreden, T.M. Ashhurst, B. Chami, D. McCarthy, H. Wu, J. Ma, A. Martin, L.D. Shae, P. Witting, G.S. Kansas, J. Kuhn, W. Hafezi, I.L. Campbell, D. Reilly, J. Say, L. Brown, M.Y. White, S.J. Cordwell, S.J. Chadban, E.B. Thorp, S. Bao, S.D. Miller, N.J. King, Therapeutic inflammatory monocyte modulation using immune-modifying microparticles, Sci. Transl. Med. 6 (219) (2014), 219ra217.

[38] C. Neyen, A. Pluddemann, P. Roversi, B. Thomas, L. Cai, D.R. van der Westhuyzen, R.B. Sim, S. Gordon, Macrophage scavenger receptor A mediates adhesion to apolipoproteins A-I and E, Biochemistry 48 (50) (2009) 11858—11871.

[39] M.S. Sulkowski, M. Kang, R. Matining, D. Wyles, V.A. Johnson, G.D. Morse, V. Amorosa, D. Bhattacharya, K. Coughlin, F. Wong-Staal, M.J. Glesby, A.C.T.G.A.P. Team, Safety and antiviral activity of the HCV entry inhibitor ITX5061 in treatment-naive HCV-infected adults: a randomized, double-blind, phase 1b study, J. Infect. Dis. 209 (5) (2014) 658—667.

[40] S. Marleau, D. Harb, K. Bujold, R. Avallone, K. Iken, Y. Wang, A. Demers, M.G. Sirois, M. Febbraio, R.L. Silverstein, A. Tremblay, H. Ong, EP 80317, a ligand of the CD36 scavenger receptor, protects apolipoprotein E-deficient mice from developing atherosclerotic lesions, FASEB J. 19 (13) (2005) 1869—1871.